

Detection of Radioactive Gas with Scintillating MOFs

Sharvane Mauree, Vincent Villemot, Matthieu Hamel, Benoit Sabot, Sylvie Pierre, Christophe Dujardin, Francesca Belloni, Angiolina Comotti, Silvia Bracco, Jacopo Perego, and Guillaume H. V. Bertrand*

Homogenous radioactive gas contamination constitutes the hardest challenge for radioprotection due to its elusive nature. Most common radioactive gas are ^{85}Kr , ^{222}Rn , and tritiated (^3H) vapors. Each of them has different challenges, often leading to specialized single-gas detectors. The state-of-the-art detection either produces chemical-radiological waste, is hard to implement online, or requires large volume. A new paradigm is presented for radioactive gas detection that can perform online detection on any gas and fit in the hand. This study uses photoluminescent metal organic frameworks (MOFs) as both porous gas sponges and scintillators. The response of several zinc based MOF is studied, using a unique radioactive gas test bench. These tests showed that MOFs are able to both concentrate and detect successfully ^{85}Kr . The investigation is completed with calibration with different activities. The study also reports detection of ^{222}Rn , and measurement of its half-life. Finally, the study is completed with the successful detection of tritiated dihydrogen, commonly known to be a hard radionuclide to detect due to its low energy and penetration range. This paper shows that scintillating MOFs are a powerful solid-state approach and a practical solution to the challenge of radioactive gas measurements.

homogeneous (mainly noble gas and tritiated gas). Heterogeneous contaminations are commonly captured with a filtration technique. It aims at depositing and concentrating the suspended contamination on a filter, thus obtaining a solid state radioactive source, which is then measured by a classical contamination meter.^[1,2] Homogeneous contaminations are impervious to this technique and need a dedicated solution. Very few technologies can efficiently perform such a detection,^[3–5] which is our focus here. To encompass this field, we will present the three “usual suspects” of homogeneous airborne contamination and the challenge they each represent.

^{85}Kr is a noble gas, which is a quasi-pure beta emitter (99.7% beta) with an average energy of 251 keV and a maximum at 687 keV. ^{85}Kr represents the majority of the manmade airborne contamination, as it is part of the nuclear fuel reprocessing cycle.^[6] Its emissions are estimated at 379 PBq/year for the La

Hague reprocessing plant in 2019 and 95 PBq/year for Sellafield reprocessing plant in 1999.^[7] To the best of our knowledge, these two reprocessing plants are the only ones to have quantified their emissions, so these are bottom values that stress out the need for a suitable detector able to monitor the exposure to ^{85}Kr in these working environments. The order of magnitude of ambient radioactivity in these facilities depends on the location: 1 kBq cm^{-3} at the mouth of the evacuation chimney as opposed to the 1 Bq cm^{-3} at the ground level of the facility and

1. Introduction

In the field of nuclear detection, airborne contamination represents a particular challenge. As opposed to liquid or solid state contamination, radioactive gases are a more elusive danger as their volatile nature makes them more challenging to contain. Because of its volatile nature, online detection is also of paramount importance to mitigate exposure. Airborne contamination can be categorized as either heterogeneous (aerosols) or

S. Mauree, V. Villemot, M. Hamel, S. Pierre, F. Belloni, G. H. V. Bertrand
Université Paris Saclay
CEA
List
Laboratoire Capteurs et Architectures Electroniques (LCAE)
F-91120 Palaiseau, France
E-mail: guillaume.bertrand@cea.fr

B. Sabot
Université Paris Saclay
CEA
List
Laboratoire National Henri Becquerel (LNE-LNHB)
91120 F-Palaiseau, France
C. Dujardin
Institut Lumière-Matière
CNRS UMR5306
Université de Lyon 1
69622 Villeurbanne CEDEX, France
A. Comotti, S. Bracco, J. Perego
University of Milano – Bicocca
Department of Materials Science
Via R. Cozzi 55, 20125 Milan, Italy

 The ORCID identification number(s) for the author(s) of this article can be found under <https://doi.org/10.1002/adfm.202302877>.

© 2023 The Authors. Advanced Functional Materials published by Wiley-VCH GmbH. This is an open access article under the terms of the Creative Commons Attribution-NonCommercial License, which permits use, distribution and reproduction in any medium, provided the original work is properly cited and is not used for commercial purposes.

DOI: 10.1002/adfm.202302877

to the natural occurrence of 1 Bq m^{-3} . Furthermore, ^{85}Kr is a classical fission product present in the atmosphere of nuclear power plants, especially in the nuclear core building. The level recommended by the European Commission and EDF (French electricity provider, who run the nuclear power plants park) in a reactor building^[8] is 1.8 Bq cm^{-3} . Continuous monitoring of ^{85}Kr concentration is not yet implemented due to the lack of an online detector able to sense these levels. Still, such an apparatus could be of paramount importance in the radioprotection of workers as well as an indicator of the core's structural health.

^{222}Rn is a noble gas and an alpha emitter of 5.59 MeV. It makes for the large majority of natural homogenous airborne contamination, as ^{222}Rn is a daughter isotope of the ^{238}U decay chain. In regions with granitic bedrock, its accumulation in closed rooms and underground is a real public health problem. ^{222}Rn is evaluated to be the second cause of lung cancer behind tobacco consumption.^[9] The World Health Organization (WHO) and the European Commission set a guideline level of 400 Bq m^{-3} for existing houses and 200 Bq m^{-3} for future dwellings.^[10] As an alpha emitter, the detection of radon cannot be performed at a distance due to its low penetrating power. This low range makes planar scintillators unsuitable for the job and, similar to tritium discussed below, emphasizes the need for volumetric detection. Reaching a low detection level is not straightforward in classical configuration (i.e., direct or indirect detection with simple geometries).

^3H (tritium) can be present as tritiated dihydrogen or tritiated water vapor. It is a pure beta emitter with an average energy of 5.7 keV and a maximum at 18.6 keV. This very low energy makes it very difficult to detect, as its maximum penetration is only 6 mm in air and $6 \mu\text{m}$ in water. This strong screening effect of the carrier gas makes most traditional sensors inefficient, with a poor effective gas volume of detection. Tritium is present in different applications; it is an activation product of the nuclear fuel cycle, the primary fuel for fusion reactors (ITER) and bombs. Its detection presents both civilian and military applications.^[11,12]

Outside of these three gases, other isotopes of interest are ^{133}Xe (pulmonary imaging) and ^{135}Xe (fission product), which have beta emission between ^{85}Kr and ^3H ; other isotopes of radon are also interesting but very close to ^{222}Rn in terms of decay chain.

As shown above, there are no common applications, sources, or decay modes for these radioactive gases. The state-of-the-art solution for radioactive gas detection is, therefore, application-driven. One can find very specialized detection devices, such as diffusion chambers with membranes, which isolate radon from the air, but for radon measurement only. The two best available technologies that could be flexible are proportional gas counters^[5] and liquid scintillation counting.^[3] Proportional gas counters can offer a delayed online detection (>20 min) but need a carrier gas, often argon-methane (explosive) or xenon (expensive). They often use oxygen exclusion techniques, adding an O_2/N_2 separation apparatus to the detector, as it diminishes the performance of the detectors. Furthermore, the counting system is quite imposing, and the need for gases adds a very bulky pressurized bottle to the setup, making it a stationary-only solution. Liquid scintillation is best for low-penetrating ionizing rays. It is the metrological standard for alpha

emissions from ^{222}Rn (thanks to radon solubility in liquid scintillators) or weak beta from tritium. However, it is not possible with ^{85}Kr due to its poor solubility in liquid scintillators. Using a liquid scintillator consists of a sampling step to dissolve the gas in a material (bubbling in water, absorption on material), making this technique impractical for online measurements and not fully reproducible due to the volatility of noble gases in the liquid scintillator. Each liquid scintillation measurement also produces liquid waste with mixed chemical and radiological hazards that are difficult to dispose of.

There is a real need for very sensitive detectors able to perform online measurements of radioactive gas. The solution we propose herein is inspired by the efficiency of the liquid scintillator regarding its interaction with a radionuclide. We can conceptualize it as similar to a radionuclide in solution, which has a maximum surface in contact with the scintillator, avoiding the self-shielding of low beta or alpha emitter. We thus turned our attention to materials with very high specific surface areas that interact optimally with gases and exhibit scintillating properties. Metal Organic Frameworks (MOFs) stand out as one of the ideal solutions for this problem as they are the class of materials with the highest specific surfaces and can be chemically designed almost at will. Since MOFs can be both the scintillator and a radioactive gas sponge,^[13] with the possibility of adsorbing, concentrating/selecting, and detecting the targeted gas, the core idea of our approach is to use all the remarkable features of MOFs to our advantage. MOFs for radiation detection have already been explored in the literature^[14–16] as scintillators dispersed in polymeric matrices,^[17–19] similar to the style of plastic scintillators. Their potential as both radioactive gas sponge and scintillators was theorized^[20] but never explored together. In this paper, we propose to take this step, demonstrating all the potential of scintillating MOFs for radioactive gas detection. We first synthesized four MOFs with complete structural and photophysical characterization. Then we recorded their scintillation properties in the presence of radioactive gas. To do so, we placed the MOFs inside a metrological device, a triple-to-double coincidence ratio (TDCR) counter,^[21] modified to be connected to a metrological radioactive gas test bench.^[22] We showed that scintillating MOFs are an extremely potent solution for detecting medium levels (35 to 250 Bq m^{-3}) of our targeted radioactive gases. This first evaluation of performances, in terms of detection threshold and response time, makes using MOFs a game changer in the field of radioactive gas detection.

2. Experimental Section

Our approach for radioactive gas detection was based on the combination of porosity and photoluminescence in MOFs. To achieve this duality, we focused on the synthesis of known MOFs with classical structural characterization for the porosity aspect (PXRD, BET, TGA). We also performed photophysical and radiophysical experiments on each of them to evaluate their properties. All the characterization can be found in the supporting information.

As our main focus is radioactive gas detection, we will present our homemade metrological test benches. The gas bench consists of various mixing lines allowing for the dilution of pri-

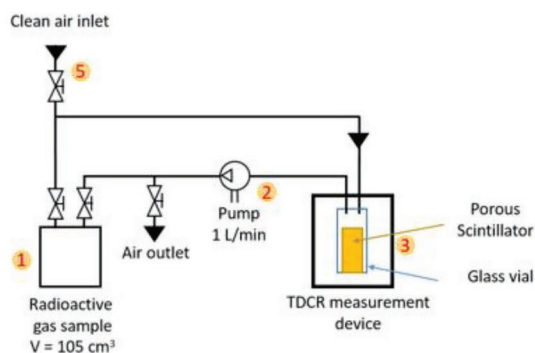
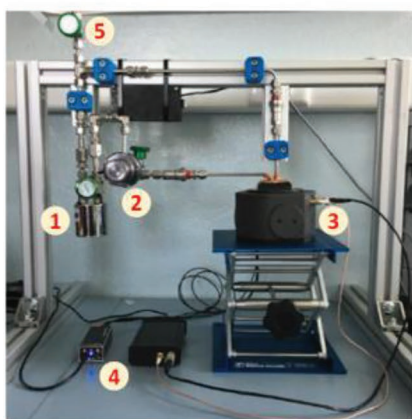


Figure 1. Top: Primary radioactive gas test bench for the generation of metrological control gas sample. Bottom left: Photo of the miniaturized radioactive gas test bench. Bottom right: Schematic representation of the system (not to scale).

mary radioactive gas standards and their easy handling.^[22] This installation enabled to produce samples whose total activity is controlled and known precisely for any radioactive gas except ^{222}Rn , which has another dedicated setup.^[23] These samples were then connected to a closed circuit (total volume of 139 cm^3), allowing the production of a radioactive atmosphere of known activity in dry, filtered air (i.e., without aerosols and relative humidity $< 3\%$). Two identical experimental setups (Figure 1) were designed, one for ^3H (contaminating gas) and one for the other radioactive gases; they consist of:

- a container (1) with a volume of 104.4 (5) cm^3 capable of containing a known activity of radioactive gases;
- a pump (2) allowing gas circulation in the system at a rate of $0.70\text{ (5) L min}^{-1}$, providing a homogenous distribution of radioactive gas in the circuit within seconds;
- a TDCR counter with a circulation vial (3) and its associated electronics (4);
- a clean air inlet and outlet (5) to purge the system.

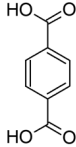
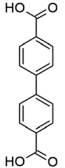
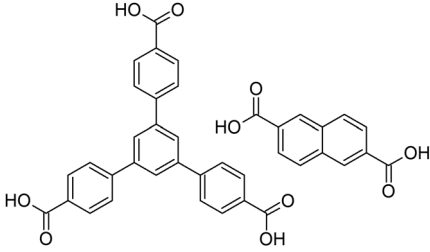
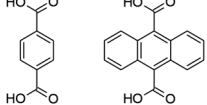
The TDCR counter was a precise metrological device, which consisted of three photomultiplier tubes (PMTs) and allowed absolute activity measurement of alpha, low-energy beta, and electron-capture radionuclides with liquid scintillation sam-

ples.^[24] This system, micro-TDCR, was developed and built at LNE-LNHB and was validated and used for various studies over the last 5 years.^[21] This micro-TDCR uses 3 PMTs with a maximum quantum yield (43%) between 280 and 420 nm. This measurement set uses specific electronics, which allowed to record the logical sum of the double coincidences (D) as well as the triple coincidences (T) between the three PMTs with an adjustable coincidence window (here 40 ns or 400 ns) and an extendable dead time of 50 μs . For the first time, the TDCR device was adapted as a circulating device to accommodate a vial with a tube in the center containing the MOF crystals. This tube was reduced to an internal diameter of 4 mm to limit light scattering from the sample and thus collect maximum information using the three PMTs.

For each experiment, the same type of sequence was carried out; the duration of each step was adapted according to the phenomena observed during the experiment (stable count rate, yield evolution, possible absorption....). These experimental sequences were divided into three steps:

- Measurement of a reference blank: circulation of clean air without additional radioactivity,
- Circulation of the radioactive gas sample (^{85}Kr , ^{222}Rn or ^3H), only one isotope mixed with air, into the vial with the

Table 1. MOFs used in this study.

MOFs names	Ligand(s)	Nodes	SI References
MOF-5		Zn ₄ O	Figures S2–S9
MOF-9		Zn ₄ O	Figures S10–S16
MOF-205		Zn ₄ O	Figures S17–S25
MOF-5-ADC		Zn ₄ O	Figures S26–S34

scintillator; the targeted activity of the sample is 10 kBq corresponding to a high activity concentration of 72 Bq cm⁻³ in the loop,

- Circulation of clean air into the device to purge the radioactive gas.

During the experiment, the logical sum of the double coincidence counting rate (*D*) of the TDCR device was followed. This *D* value could be observed at two different coincidence windows, 40 ns or 400 ns. The triple coincidence (*T*) was measured and deduced the efficiency indicator (*T/D*), which in a perfect case has a value of 1, meaning 100% detection efficiency. From these results, we could deduce if we have radioactive gas detection, its detection efficiency, adsorption, desorption, or other phenomena.

To explore the capacity of MOFs to efficiently interact with radioactive gas, the MOFs were activated under vacuum and temperature before being placed inside the experiment vial. Our best candidates were also characterized more thoroughly with the help of solid-state and hyperpolarized Xenon NMR.

3. Result and Discussion

3.1. Scintillating MOFs Library

Fluorescent MOFs are widely known in the literature,^[25–27] and numerous ligands used in these MOFs are also found in classical organic scintillators.^[28,29] We focused our synthetic efforts

on MOFs containing aromatic conjugated structures (Table 1). We chose as a baseline MOF the iconic MOF-5, which can exhibit a fluorescence between 350 nm and 450 nm depending on its hydration state.^[30] We then extended toward the iso-reticular structure with IRMOF-9, a concatenated MOF based on a biphenyl unit. MOF-205 was also synthesized, as it is a two-ligand system based on a triphenyl benzene and a naphthalene building block. The latter is very interesting as it is often used in liquid scintillators for its photophysical characteristics (decay time, wavelength, quantum yields...).

We also explored a last avenue to make scintillating MOFs: partial ligand doping. As described in the literature,^[31] it is possible to replace small quantities of a ligand with another sharing the same size and chelating groups. This is a way to introduce distinct ligands in a stable but poorly fluorescent lattice to improve the optical properties of known MOFs without altering their structures. Hence, we synthesized and tested MOF-5 derivatives doped with 9,10-anthracene dicarboxylic acid (ADC), named here MOF-5-ADC.

3.2. Photophysical Characterization

Each of the synthesized MOFs was targeted because of their fluorescence properties. All these analyses are available in the SI, but we will present the case of our doped MOF here. MOF-5 is an iconic material that is easy to produce and has known fluorescence properties^[30] that depend on its hydration level and structural integrity. Pure anhydrous MOF-5 has a very

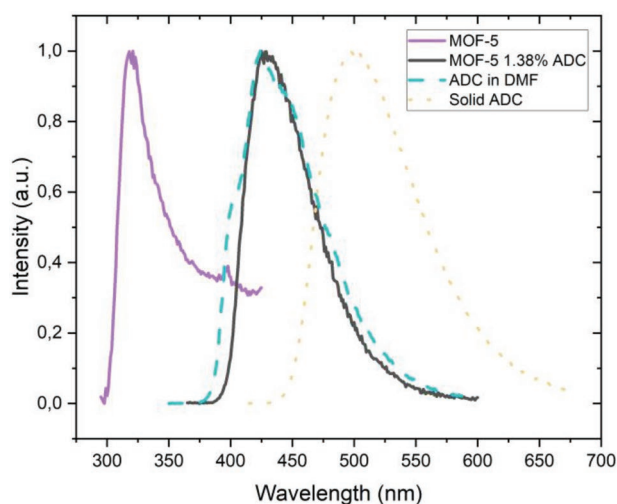


Figure 2. Photoluminescence spectra of MOF-5 and MOF-5 doped with ADC, and its comparison with ADC as a solid or in solution

low fluorescence yield and an emission centered at 350 nm (FWHM \approx 100 nm). The insertion of a small percentage (1.38 %) of 9,10-anthracene dicarboxylic acid in its lattice reminds us of the standard strategy with plastic scintillators to dope a styrene matrix with efficient fluorophores.^[28]

In **Figure 2**, we present the photoluminescence (PL) of undoped and doped MOF-5. The effect of this doping is visible with the shift of the emission wavelength (**Figure 2**). This emission wavelength of MOF-5-ADC is more suited for scintillation set-ups, as traditionally, PMTs have a maximum efficiency of detection \approx 420 nm. The emission of MOF-5 (350 nm) is centered on the ligand present in the structure since the metal, Zn, has a d^0 full shell electronic configuration. Our team has also experimentally demonstrated this previously in ref. [31] Upon adding the 9,10 ADC ligand to the MOF, the wavelength of emission shifts to higher wavelength and is now centered on the ADC ligand as shown in **Figure 2**. Even though the BDC ligand is still higher in proportion in the MOF-5-ADC structure, the fluorescence yield of the ADC is higher than that of the BDC and therefore the fluorescence of the ADC will overpower that of the BDC, hence centering the overall emission of the MOF on the ADC. Each MOF was also tested in a radioluminescence experiment with X-rays as the excitation source, and the results are also presented in the SI.

3.3. MCNP-6 Simulation

Monte-Carlo simulations were performed to evaluate the proportion of beta decay from ^{85}Kr that escaped from our sample container without interacting with the MOF and are detailed in the SI.

3.4. Solid State and Xenon NMR Experiments

As **Figure 4** will later show us, MOF-205 and MOF-5-ADC are our most promising candidates for the detection of radioactive

gases. Powder XRD of the activated MOF-5-ADC and MOF-205 show high crystallinity (**Figures S17 & S26**, Supporting Information) and profiles corresponding to the known crystal structures, as observed by comparing the experimental to the calculated powder patterns and according to their cubic structures with space groups Fm-3m and Pm-3n, respectively.^[32,33] The cubic crystal structure of MOF-5-ADC comprises octahedron-shaped Zn_4O clusters as secondary building units connected by terephthalate ligands, thus forming intercommunicating cavities. MOF-205 is constructed by two distinct ligands, trifunctional tris-carboxybenzyl-benzene and bifunctional dicarboxylate naphthalene, coordinated with Zn_4O cluster, and contains dodecahedral and tetragonal interconnected pores.

^{13}C magic angle spinning (MAS) experiments confirm the stoichiometry of the MOFs and the absence of any signal which could pertain to residual solvents. ^{13}C CP MAS NMR spectra of MOF-5-ADC show three narrow signals according to the ligand structure and symmetry, whilst MOF-205 CP-MAS NMR spectra display two resonances at \approx 175–176 ppm assigned to the carboxylate groups of the two ligands and a multiplicity of signals in the aromatic region in agreement with the independent carbon atoms in the unit cell. The fully relaxed ^{13}C MAS NMR spectrum of MOF-205, collected with 60s recycle delay between pulses, confirms the relative ratio of the two ligands (2:3 trifunctional vs difunctional-based ligands) in the crystal structure.

The porosity of both MOFs samples was tested by N_2 adsorption isotherms at 77 K. The results show high surface areas of 3752 (Langmuir) and 3344 $\text{m}^2 \text{g}^{-1}$ (BET) for MOF-5-ADC and 5390 (Langmuir) and 4350 $\text{m}^2 \text{g}^{-1}$ (BET), which are among the best values published for this MOFs.^[32,33] As calculated by Non-Linear DFT and carbon slit pore model, the pore size distribution was centered at 12.5 Å for MOF-5-ADC while two maxima at 13.5 Å and 17.3 Å were observed for MOF-205, in agreement with the pores predicted by the crystal structures.

The accessibility of the pores to the gas phase under a flow of a noble gas such as Xe was demonstrated by Continuous Flow Hyperpolarized (CW-HP) ^{129}Xe NMR, which is a laser-assisted technique enabling to detect a signal of the diffused gas into the cavities at high resolution. The optical pumping technique achieves high sensitivity (hundreds of times the signal intensity detected under thermal conditions) even with a low 1–2% concentration of Xenon in a gas mixture with 94% He and 4% N_2 .^[34,35] The experiments, performed at low partial pressure, ensure that intermolecular interactions of Xenon with the framework prevail, while Xe-Xe interactions are negligible. Thus, the Xenon chemical shifts depend only on the distinct environments of Xenon confined in restricted spaces. Remarkably, such signal can be observed after only a few ms ($<$ 200 ms) after the contact of the gas with the porous materials. Notably, the CW-HP ^{129}Xe NMR spectra of the two MOFs at room temperature show two predominant signals in the region at \approx 50 ppm for MOF-5-ADC and 45 ppm for MOF-205 that are different from the free gas (at 0 ppm), indicating a fast diffusion of Xenon atoms in the confining cavities. The downfield resonances demonstrate that Xenon atoms are interacting with distinct adsorption sites in the cavities, specifically; at such a low Xenon concentration, the primary interactions are expected with the metal nodes, as already observed for other gases such as argon.^[36,37] When lowering the temperature, both the signals

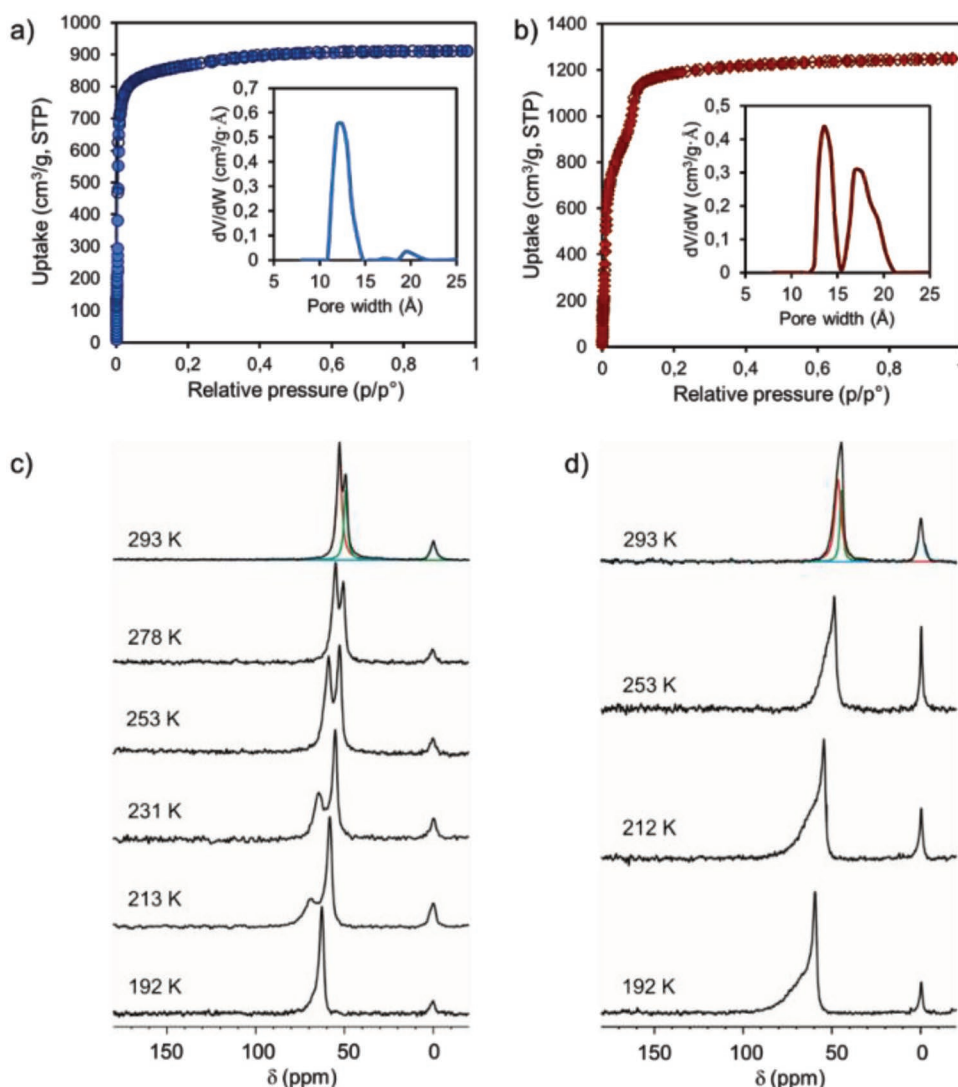


Figure 3. N_2 adsorption isotherms at 77K of MOF-5-ADC (a) and MOF-205 (b). In the insets pore size distribution as calculated by Non Linear NL-DFT and carbon slit pores. CW-HP ^{129}Xe NMR spectra of MOF-5-ADC (c) and MOF-205 (d) as function of temperature. The peak at 0 ppm corresponds to the free Xe.

shift to higher chemical shifts, suggesting a stronger interaction with the walls of the host. This result is presented in Figure S39 (Supporting Information) where each signal is fitted via a peak splitting in order to isolate both chemical shift.

In the CW-HP ^{129}Xe NMR spectra of the MOF-5-ADC and MOF-205, the predominant signals at the region of 40–80 ppm gradually change from one to two peaks as the temperature increases. This phenomenon is due to MOF-5 and MOF-205 having both two different pore in term of interaction with Xe. What we are observing in the CW-HP ^{129}Xe NMR experiment is the variation of interaction from a xenon atom. At low temperature, the Xe move slowly and are able to interact in specific way in each type of pores. When temperature increases, this interaction become more and more similar due to molecular agitation.

Xenon is an intermediate element on the column of the periodic table with respect to the radioactive targeted noble gases (^{85}Kr and ^{222}Rn) under study. Thus, this experiment performed

under a continuous flow of Xenon and at room temperature directly demonstrates the absorption of noble gas within the two frameworks **Figure 3**.

3.5 Exposure to radioactive gas. As mentioned above, our targets are ^{222}Rn , ^{85}Kr , and ^3H . Each gas has its specificity, described in the introduction. ^{85}Kr was chosen to screen the performance of all scintillating MOFs because it has a quasi-pure beta emission (99.7%) with relevant energy and a stable isotope daughter. As a first approach, this will give more signal than the low energy beta of the tritium and more ease of interpretation compared to the complex decay chain of the ^{222}Rn (Figure S1, Supporting Information). It also has a lesser contamination potential than tritium; therefore, samples would be readily reusable for different test runs. Once the entire tests were completed, the sample was used in the second test bench for tritium experiments.

^{85}Kr exposure: ^{85}Kr produces charged beta particles with a maximum energy of 687 keV; this implies the generation of

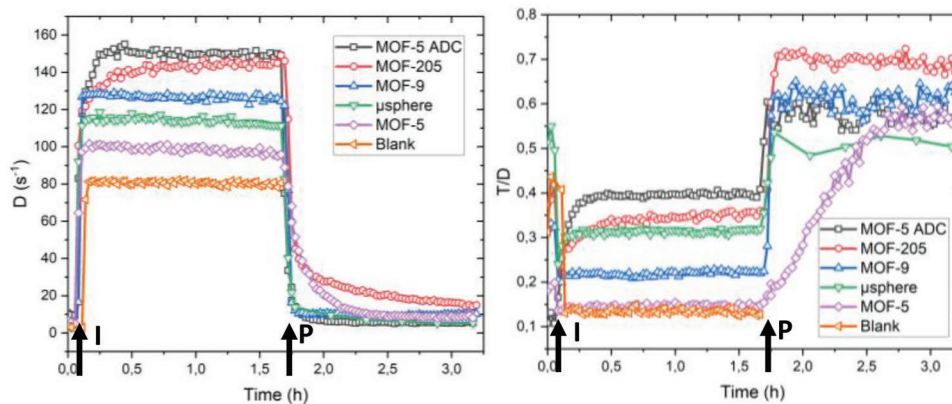


Figure 4. Left: Count rate of different substrates exposed to a ^{85}Kr atmosphere. Right: Associated TDCR yields. I = Injection of radioactive atmosphere P = Purge with dry air

Cherenkov light in the glass walls of our vials. The Cherenkov Effect is anisotropic, which makes it harder to detect by our triple coincidence setup. Nevertheless, diffusion/reflection phenomenon can occur, and thus a background of Cherenkov light is observable when an empty vial is used in the system (Figure S37, Supporting Information). A very weak T/D indicator (Figure S38, Supporting Information) also characterizes the Cherenkov background, which is explained by its anisotropic nature. This control procedure enables the evaluation of the real impact of subsequent loading with the samples.

The closest to a porous scintillator found in the literature are scintillating microspheres developed by Tarançon et. al.,^[38] which present the highest surface/volume ratio tested for solid scintillators. These microspheres also exhibit a small permeability toward gas.^[39] We choose these scintillating microspheres as another point of reference. The experiments showed that their response is higher than the blank measurements, hence validating its use for the detection of radioactive gas.

For all the MOFs samples, the same experiments were performed as described in the method section by using a well-known activity concentration from the same activity standard. As mentioned, each MOF sample was activated by solvent exchange followed by a vacuum and temperature treatment. The MOFs were then stored in a glovebox before being characterized on the gas bench. Due to the exposition to nitrogen from the glovebox and the use of dry air as a carrier, we consider the pore of the MOFs already filled. Therefore, our working hypothesis relies on the diffusion and uptake of radioactive gas in the pores. Strong of numerous literature reports on MOF selectivity,^[40] we were also expecting other effects to influence the measurements:

- The first concerns the affinity of certain gases with certain MOFs allowing them to concentrate the gas inside the pores, making a local increase of its concentration, and thus activity in the case of a radioactive gas; this effect is labeled as a concentrator effect.
- The second is the difference in the diffusion dynamic of gas inside the porous architecture, which will dictate the dynamic of the system at the injection but also at the purging step with potential gas retention.

After injection and circulation of the radioactive gas, the system was allowed to reach equilibrium, corresponding to a plateau observed in the D count rate. Then the whole system was purged with the circulation of dry air.

As presented in **Figure 4**, all the tested MOFs presented a count rate superior to the blank, which indicates that more photons are detected than a pure Cherenkov effect. To ensure that the photons are coming from a scintillation mechanism, one last control is necessary. One possibility is that our fluorescent MOF acts as a fluorescence shifter, absorbing the unidirectional Cherenkov emission and reemitting it isotropically at a longer wavelength better suited for the PMTs. This possibility was discarded with a control test of our best counting sample (MOF-5-ADC) but with the sample holder's cavity plugged. This experiment (Figure S36–S38, Supporting Information) produced the same counting rate and T/D indicator as the empty control experiments without a plug, showing that Cherenkov shifting is negligible in our systems. Thus it confirms that every count rate above the Cherenkov blank can be attributed to scintillation due to the interaction of the radioactive gas radiation with the MOFs samples. With this control experiment in mind, the results show that MOF-5 is worse than the reference scintillating microspheres but that MOF-9, MOF-205, and MOF-5-ADC are increasingly better in terms of count rate, hence validating our doping approach to make scintillating MOFs. This difference in performances can be explained by a combination of factors. At first a difference in scintillation yield (proportional to TDCR yields **Figure 4** right) explains the order between MOF-5 ADC, MOF-205, the microspheres and the blank test. But MOF-9 seems to have a lower yield but a better count rate than the microspheres, we explain that by its ability to adsorb the ^{85}Kr and increasing its local concentration. This phenomenon is also present for MOF-5 ADC and MOF-205 and is detailed below.

One can note that in the right channel of **Figure 4** the baseline before and after the test has increased significantly. The increase of the baseline can be due to the retention of some gas in the MOF. However, we can see during the measurement in **Figure 5**, where the purging was performed for a longer time that the baseline always returns to the same level given enough time for the gas to leave the pores of the MOF

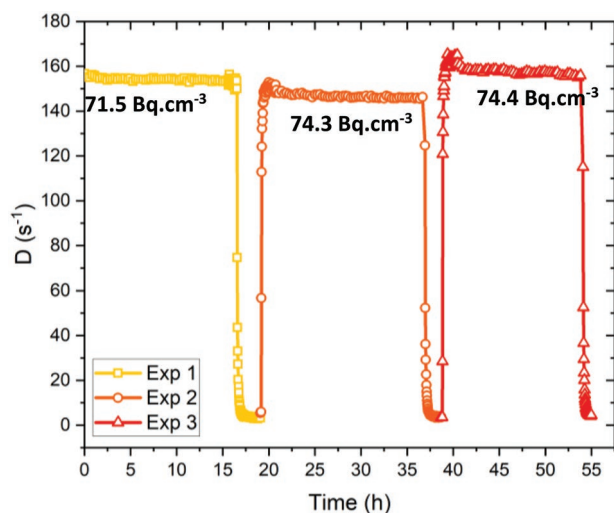


Figure 5. Count rate reproducibility and long-time exposure experiments of MOF-205 against ^{85}Kr .

As stated before, the count rate mainly depends on the scintillation efficiency and its wavelength in regards to the optimal PMT quantum efficiency. Our best MOFs with the highest counting rate from this screening are MOF-205 and MOF-5-ADC. This is coherent as they are the two MOFs with the emission profile the closest to the PMT maximum efficiency (40 % between 280 nm and 420 nm). With the shorter TDCR coincidence window (40 ns), MOF-205 and MOF-5-ADC give D count rates of 170 s^{-1} and 200 s^{-1} , respectively, when exposed to a flux of ^{85}Kr . This value can be subtracted from the Cherenkov blank to give us 70 s^{-1} and 100 s^{-1} from pure scintillation phenomena for our two best MOFs. With the volume of the sample holder, we can deduce a primary efficiency of detection for ^{85}Kr exposure.

$$\varepsilon_D = \frac{D}{A_V \times V} \quad (1)$$

Where ε_D is the primary detection efficiency, D is the net count rate in s^{-1} (blank and Cherenkov count rate being subtracted) observed on the average of the logical sum of the double coincidence plateau, A_V is the injected volumic activity in $\text{s}^{-1}\text{ cm}^{-3}$, and V is the volume of the cavity of the sample holder in cm^{-3} . The ε_D values for the MOFs are represented in Table 2.

These ε_D values are the first indicator of the performances of our samples and are already above 100 %. This is evidence of an awaited concentration effect of our MOFs, meaning that ^{85}Kr would preferentially interact inside the pores and have a local concentration inside the MOFs superior to the injected one.

Table 2. Parameters and efficiency for MOF-205 and MOF-5-ADC.

	Cps	A_V	V	ε_D (%)	ε_c (%)
MOF-205	70	74.6 Bq cm^{-3}	0.5 cm^3	188	207
MOF-5-ADC	100	75.7 Bq cm^{-3}	0.5 cm^3	264	334

The first approach to correct this ε_D efficiency is to estimate the true volume accessible to the gas since the MOF occupied a specific volume in the cavity of the sample holder as well as the true activity that interacts with the MOFs. Given that these two values are overestimated here, the primary efficiency presented here is a lower value of the system's true potential.

With the knowledge of the MOFs' mass we put inside the cavity (181 mg and 161 mg, respectively, for MOF-205 and MOF-5-ADC) and the theoretical density of our MOFs (0.3 and 0.2 respectively),^[41] we can evaluate the percentage of the occupied volume by MOF-205 and MOF-5-ADC at 47.6% and 40.0% respectively. As MOFs are porous architectures, this volume must be corrected by the percentage of the void present in these architectures. This correction was calculated using lattice parameters and experimental pore size, obtained by BET, to obtain a percentage of the MOF actually occupied by matter. The values are 21% and 52% for MOF-205 and MOF-5-ADC. This gives us a final volume occupied by the MOFs of 9.52% and 20.8%, respectively, percentages that need to be deduced to access the corrected volume (V_c).

We also performed MCNP-6 simulation to estimate the percentage of beta that interacts with our system. Our MOFs are not very dense, therefore, there is a possibility that beta escapes and does not interact with our scintillating MOFs. The simulation provides us with a 99.7% proportion of beta that interacts and deposits at least 1 keV inside the MOF. Therefore, only 0.3% of the beta from ^{85}Kr decay are not seen by our system, so the corrected volumetric activity (A_{Vc}) is comparable to the uncorrected one.

With these corrected values V_c and A_{Vc} , we can infer a corrected efficiency that comes a little closer to the true efficiency of our system:

$$\varepsilon_c = \frac{D}{A_{Vc} \times V_c} \quad (2)$$

These ε_c efficiencies are not yet true efficiency measurements as several parameters such as scintillation yields, transparency of the media, or nonlinearity of the scintillator are not considered. For example, in case of very low energy interaction, only a few photons will be emitted, so the probability of registering a coincidence event will diminish. These effects in the case of ^{85}Kr are negligible because of its relatively high beta spectrum, hence are not explored here.

This gave us an efficiency of 207% for MOF-205 and 334% for MOF-5-ADC. Once again, efficiency over 100% is a notable thing that we expected and explain by the nature of the MOFs with their ability to interact favorably with the targeted gas, hence artificially concentrating it inside them. This concentration effect increases the number of radioactive atoms inside the pores of our MOFs, thus inflating the count rate and the efficiency of our system. This validates our hypothesis that MOFs porosity is a game-changer for noble gas low-level activity measurements.

The D count rate and the T/D indicator obtained with the MOFs were continuously observed (Figure 4) as the system was purged with dry air. The combined analysis of these two values gave us a strong indication of the capacity of our MOFs to trap

the ^{85}Kr . The general analysis of a result can be broken down as follows:

1. First step: Baseline measurements before ^{85}Kr injection. The measurements give a low count rate due to external interactions (muons, natural radioactivity, ...) in the scintillating material with a fluctuating but stable T/D value over time (fluctuation due to low statistics). This step is here to determine our baseline.
2. Second step: injection of ^{85}Kr , the T/D value changes in seconds after injection; it is generally different from the blank and depends on the detected radiation (low or high energy) and the scintillator (its scintillation yield, including the light collection). In our case, the T/D just after injection quickly reaches a low value characteristic of the Cherenkov effect. It then increases slowly over 10 minutes due to the better yields of the scintillation process as the gas diffuses inside the scintillating MOF.
3. Third step: the ^{85}Kr has circulated in the loop, and the T/D and the count rate D reach a horizontal plateau. The T/D comes from both the scintillation of the MOF (good efficiency) and the Cherenkov effect due to the high-energy charged particles interacting in the glass of the vials (low efficiency).
4. Fourth step: clean air is circulated into the loop; the T/D value increases because ^{85}Kr that is not trapped in the MOF is removed, so the Cherenkov effect disappears and the photons come from the scintillating MOF directly (higher efficiency). If the count rate D decreases slowly simultaneously, this means a dynamic of desorption is observable and comes from the MOF itself.
5. Last step: after a long air cleaning process, if T/D is maximum and the D count rate is higher than the blank, this means that a small amount is trapped into the material and that we are measuring the scintillation from the MOF. On the contrary, if the T/D and D come back to a similar value to that of step one, the radioactive gas has spread out, and the MOF is back to normal.

As shown in Figure 4, some MOFs released their load in a few seconds whereas others exhibited a slower dynamic of desorption. MOF-5 exhibits the slowest desorption. The case

of MOF-205 is also interesting as it shows a mixed desorption dynamic with at first a rapid decrease of the counting rate, but reaching a very shallow slope that indicates remaining but unknown quantity of ^{85}Kr strongly adsorbed inside the MOFs. This can be interpreted since the MOF-205 has two sizes of pores inside its lattice 13.5 Å and 173 Å. The smallest one could be responsible for this particularly long desorption process.

The study of the count rate during the purge is also fascinating as we expect a quasi-instantaneous purging of the volume not occupied by the MOF sample, thus extinguishing all Cherenkov contribution. As explained above, the Cherenkov Effect is anisotropic and therefore has a very poor T/D indicator evaluated at 0.15 in the control experiment (Figure 4 blank). During the plateau, the measurements of the T/D indicator are a combination of both Cherenkov radiation and scintillation from the MOF. This T/D value was evaluated at only 0.35 for both MOF-205 and MOF-5-ADC. Once the Cherenkov Effect is extinguished by purging with dry air, we found ourselves only with the scintillation contribution from the MOF and an increased T/D indicator of 0.72 for MOF-205 and 0.55 for MOF-5-ADC. This high T/D is another testimony of the potency of MOFs as scintillators. To explore the potential of our system, we performed a series of experiments with ^{85}Kr .

In Figure 5 we demonstrated the reproducibility of the measurements. Three active atmospheres of ≈ 10 kBq were loaded in succession with intermediate purging of the system and with the same MOF-205 sample inside. The exact activity of each active load was previously measured and then compared to the count rate. The variation of the counting rate from these three measurements corrected by the activity gives us a first evaluation of the reproducibility of the response of the sample with a standard deviation of 0.6%.

Our next step was to determine the response of our system towards different activities. In this endeavor, we used the full range of activity our test bench could make for a sample, which is from 0.202 kBq to 31.69 kBq per sample. If we consider the volume of our system, this is equivalent to 1.35 Bq cm^{-3} – 211.2 Bq cm^{-3} . The results of these experiments are shown in Figure 6. We can extract two key pieces of information from this study. First, if we plot the plateau average against the injected activity (Figure 6 right), we obtain the response function of our system. On this experimented range, the system

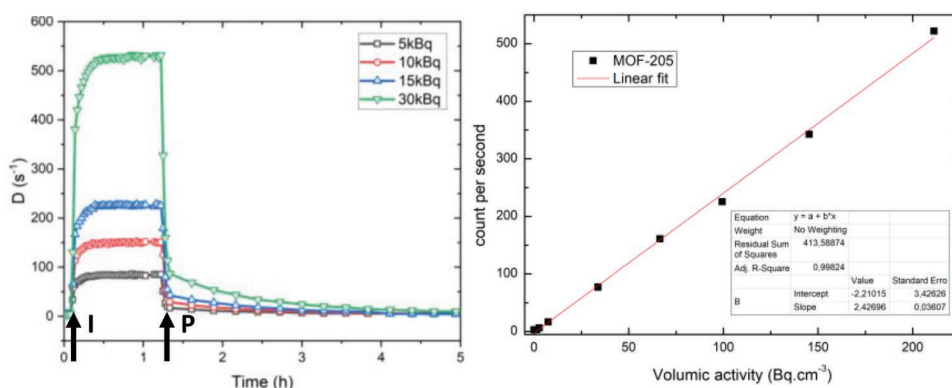


Figure 6. Left: Count rate given by MOF-205 when exposed to atmosphere with different activities of ^{85}Kr . I = Injection of Radioactive Atmosphere P = Purge with dry air. Right: average count rate of the plateau plotted against the injected activity and the associated linear fit.

Table 3. Comparison of the main technologies used for radioactive gas detection versus the one presented in this study.

	Liquide scintillation	Proportional gas counter [Air] ^[43]	Proportional gas counter [Sealed Xe] ^[44,45]	Scintillating MOF + RCTD	Required value
Limit of detection (LD)	0.005 Bq.cm ³	0.01 Bq.cm ³	0.5 Bq.cm ³	6.07 Bq.cm ³	1 Bq.cm ³
Decision threshold	0.002 Bq.cm ³	0.002 Bq.cm ³	0.1 Bq.cm ³	3.03 Bq.cm ³	0.5 Bq.cm ³
Measurement time range	1 h – 1 day	20 min – 1 h	> 1 h	1 min – 20 min	1 min
Active volume	1 L	8 L	11 L	0.8 mL	–
Final detector mass	> 100 kg	50 kg	220 kg	800 g	< 1kg
Operational practicality	Offline, fixed, mixed chemical and radioactive waste	Online, fixed	Online, fixed	Online, Portable	Online

gives a remarkable linearity, which is another advantage to our approach. This also shows that the MOF-205 response is not saturated at high activity. Nonlinearity is expected at higher injected activity, but 211.2 Bq.cm⁻³ is the upper limit of our ⁸⁵Kr source generation capacity. On the other side of the concentration range, we have the lowest activity point that cannot be differentiated from the blank measurements. Our linear fit combined with statistical^[42] analysis of our control count rate shows that our system has a decision threshold at 3.03 Bq.cm⁻³ and a limit of detection at 6.07 Bq.cm⁻³. This will be a particular focus in the future, as it will reach a level compatible with the hardest industrial regulation (limit of detection at 1 Bq cm⁻³). Data to compare our results to the classical technologies used for this application are presented in **Table 3** and show that this first study has already met the expectation for numerous practical parameters and is very close to the recommendation in terms of the detection limit. Liquid scintillation is unbeatable in term of precision, but we make for it in term of practicality and measurement time. With effort on the scintillating MOF design, we can already challenge the proportional gas counter in all aspects. In addition, as a final comment on this table, if we report all performances in regard to the active volume or detection time, the scintillating MOF is the best in all categories.

²²²Rn exposure: The same setup configuration was used to test our two best MOFs with ²²²Rn (MOF-205 and MOF-5-ADC, **Figure 7**). The decay chain of ²²²Rn contains 3 alpha and 2 beta emitters at the equilibrium considering the ²¹⁰Pb as stable due to its long half-life (of 22.23 years) compared to our experiment's time (up to 3 days) (Figure S1 Supporting Information). The total interpretation of the response with Radon is however complicated due to the fact that its decay products are solid isotopes of lead, bismuth, and polonium, so they act differently compared to gases. The decay data from the Decay Data Evaluation Project^[46] allows us to calculate a secular equilibrium time of 4 h. These two pieces of information are relevant, as they will set a minimum exposition time of 4 h in order to have a stable repartition of the different emitters' contributions inside the MOF.

Following our methodology for ⁸⁵Kr, we also performed here a blank measurement without MOFs and a measurement with scintillating plastic microspheres. The first blank is here to evaluate the Cherenkov contribution of the beta but also the photoluminescence possibility of N₂ excited by alpha particles.

This “air” component of our system is considered and presented in **Figure 7** – blank. This shows a maximum *D* count rate of 3800 s⁻¹ at 4 h, corresponding to the secular equilibrium of ²²²Rn. This is followed by a steady decrease in the count rate that can be attributed to the decay of ²²²Rn and its decay products. The *T/D* ratio for these measurements is relatively high, 0.53, compared to those of ⁸⁵Kr experiments (Figure 4). This implies a small contribution of Cherenkov and a majority of detected events from the N₂ luminescence. The control experiment with scintillating microspheres showed a slightly lower count rate but a higher *T/D* indicator. We attribute the lower count rate to highly diffusive behavior of the microsphere which tends to favor optical self-adsorption and thus diminishes the effective light output. The filling factor of the microspheres that slightly reduces the volume available to the gas could also explain a lower total activity of radioactive gas in the chamber hence a lower count rate. Nonetheless, the higher *T/D* indicator (Figures S40–S43, Supporting Information) showed that efficient scintillation phenomena are occurring. This is also valid for our two MOFs, which exhibit strong response due to scintillation, doubling the count rate compared to the blank.

Furthermore, the relatively short lifetime of the ²²²Rn can also be identify in our system, which confirms the observation

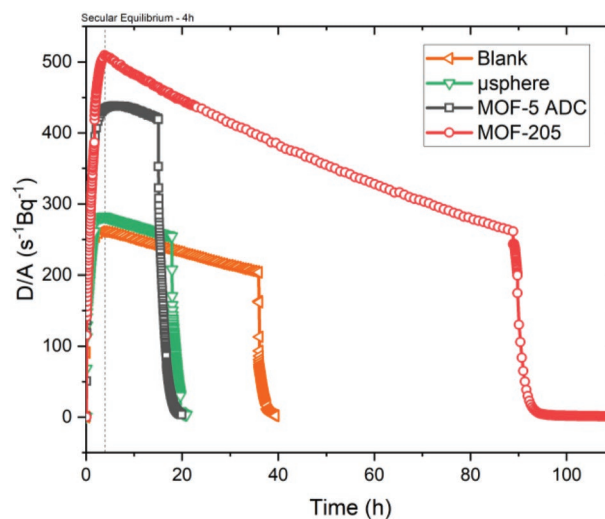


Figure 7. Count rate of different substrates exposed to an atmosphere of ²²²Rn. The dotted line at 4 hours represent the secular equilibrium.

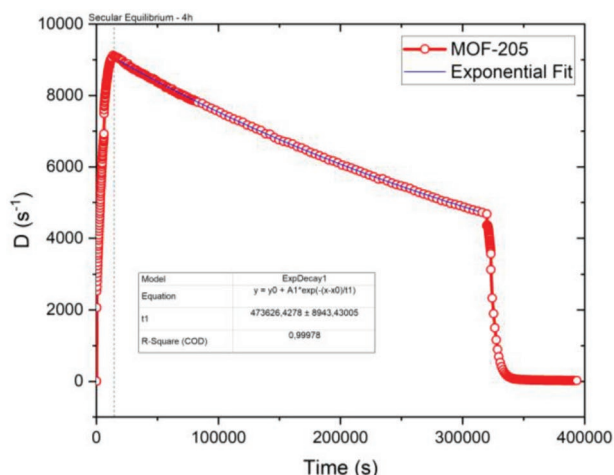


Figure 8. MOF-205 count rate evolution with respect to time during long exposure to ^{222}Rn and the associated exponential fit for the half life measurements of ^{222}Rn . The dotted line at 4 hours represent the secular equilibrium.

of the targeted gas. A longer experiment (**Figure 8**) was performed and gave us a half-life of Radon of 3.7995 days. This value is obtained by exponential fit after the secular equilibrium. It is 0.62% away from the official one: 3.8232 days,^[47] but it is the first time such a half-life is measured using a solid porous medium.

Tritiated dihydrogen Exposure: Tritium is the most challenging radioelement to test in our system, as it contaminates the entire piping and requires extensive cleaning post-measurement to avoid contamination of the following measurements, as well as accidental release. To mitigate such problems, we are working here with HT gas inside pure nitrogen. Furthermore, tritium's beta decay has a very low energy (average 5.7 keV, max 18.6 keV), hence generating very few photons for each interaction. So far, with the best liquid scintillator (e.g., toluene containing 2,5-diphenyloxazole (PPO) and 1,4-bis(5-phenyloxazol-2-yl) benzene (POPOP)) mixed with organic tritiated compound, the TDCR device we use gives a maximum of 0.76 for the T/D indicator in comparison to 0.54 with a commercial scintillator and tritiated water.^[21] However, even for low energy, the detection efficiency is not negligible as we are set to unique photon detection with the TDCR device. This is where the choice of TDCR measurements shines: we

can reliably say that slight variations in the count rate are significant and not statistical errors. Here also, MOF-205 and MOF-5-ADC were tested and compared to a blank experiment (**Figure 8**). As tritium is a pure, low-energy beta emitter, neither Cherenkov nor air contribution are expected. As expected, the blank counting rate did not change upon injection of $70 \text{ kBq}\cdot\text{cm}^{-3}$ of the radioactive gas. But for MOF-205 and MOF-5-ADC, an increase of 2.02 cps and 0.99 cps were respectively observed. Upon purging, the count rate comes back to its initial value, showing no observable adsorption of the tritium inside the MOFs. If we compare those count rates with the activity present inside the sample cavity (0.5 cm^3) we can deduce a detection efficiency for MOF-205 and MOF-5 ADC which are respectively 5.8% and 2.8%. This value seems to be low in comparison with liquid scintillation (40 – 50% efficiency)^[48,49] but it is relatively on par with diffusion chambers (5 – 14% efficiency).^[50]

As opposed to ^{85}Kr and ^{222}Rn , the detection of tritium is very weak in terms of count-rate, but nevertheless successful. We are still far away from the efficiency of liquid scintillation, but one can note the rapid response time of our system, which is in the range of minutes. This is a remarkable achievement considering the length of traditional measurements, which make tritium often considered as the most difficult commonly occurring radioisotope to measure **Figure 9**.

4. Conclusion

Following previous reports in the literature that uses MOFs as scintillators embedded in plastic matrices, we demonstrate here that fluorescent MOFs are a very potent solution for the detection of radioactive gas. This dual approach, using MOFs as both scintillators and gas sponges, was built on screening several candidates on a unique TDCR setup that allowed us to manipulate various radioactive gases. This enables us to test the three most important radioactive gases in terms of societal impact (^{85}Kr , ^{222}Rn , and hard-to-detect ^3H). The first screening put forward two candidates as efficient scintillators: MOF-205 and MOF-5-ADC. These two MOFs were then extensively characterized by solid-state and xenon NMR. These samples were tested extensively on ^{85}Kr and demonstrated a remarkable reproducibility and linearity of response. Furthermore, their high efficiency justifies our hypothesis of a concentration effect

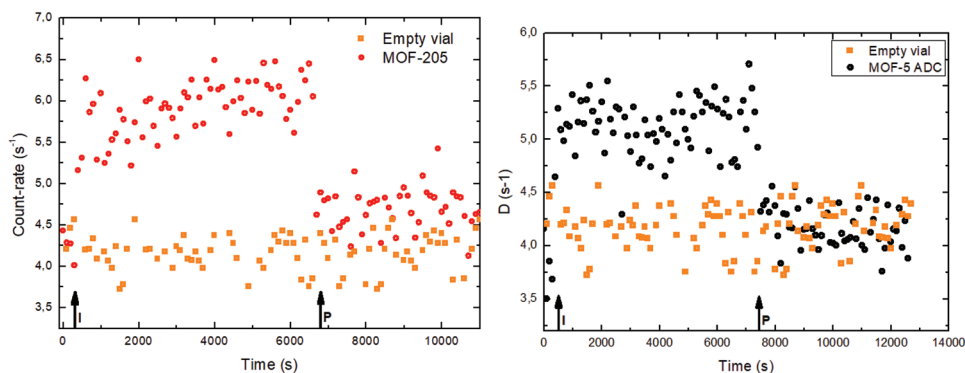


Figure 9. Count rate of MOF-205 (left) and MOF-5-ADC (right) when exposed to HT. I = Injection of radioactive atmosphere P = Purge with dry air.

inside the MOFs. As ^{85}Kr represents the majority of the man-made emission, our system would already be the only online detection solution able to follow its emission from a reprocessing nuclear fuel plant chimney. MOF-205 and MOF-5-ADC also gave successful results for the detection of ^{222}Rn with the observation of its half-life. Finally yet importantly, tritiated dihydrogen was also counted with our scintillating MOFs. These breakthrough results validate our approach and pave the way toward a new paradigm in the detection of radioactive gas with porous scintillators and, hopefully, a breakthrough in their controlled emissions. Future research will focus on lowering the limit of detection, as we are just an order of magnitude away to be compliant with environmental policy.

Supporting Information

Supporting Information is available from the Wiley Online Library or from the author.

Acknowledgements

This project has received funding from the European Union's Horizon 2020 research and innovation program under grant agreement no. 899293. This document reflects only the authors' view and the Commission is not responsible for any use that may be made or the information it contains. Sergio Piva is acknowledged for his contribution to HP Xe NMR experiments.

Conflict of Interest

The authors declare no conflict of interest.

Author Contributions

S.M. and V.V. contributed equally to this work. All the authors have contributed to the manuscript writing and proofing. Sharvane Mauree, Vincent Villemot contributed to the MOFs synthesis and characterizations. Sharvane Mauree, Vincent Villemot, Benoit Sabot, and Sylvie Pierre contributed to the radioactive gas experiment. Silvia Bracco, Jacopo Perego, and Angiolina Comotti contributed to Nmr experiment and its associated interpretation. Francesca Belloni contributed to MCNP-6 simulation. Christophe Dujardin contributed to Radio luminescence experiment and project management. Matthieu Hamel, Benoit Sabot, and Guillaume H. V. Bertrand contributed to data interpretation and project management.

Data Availability Statement

The data that support the findings of this study are available in the Supporting Information of this article.

Keywords

metal organic frameworks, radioactive gas detection, scintillation

Received: March 14, 2023
Published online: April 17, 2023

- [1] T. Mamuro, A. Fujita, T. Matsunami, K. Yoshikawa, T. Azuma, *Nature* **1962**, 194, 643.
- [2] D. F. Measday, E. C. Y. Ho, in *Nuclear Instruments and Methods in Physics Research, Section B: Beam Interactions with Materials and Atoms*, **2004**, Vol. 213, pp. 464–468.
- [3] X. Hou, *J. Radioanal. Nucl. Chem.* **2018**, 318, 1597.
- [4] C. Varlam, I. Stefanescu, O. G. Dului, I. Faurescu, I. Popescu, *Appl. Radiat. Isot.* **2009**, 67, 812.
- [5] X. Tuo, K. Mu, Z. Li, X. Li, in *Journal of Nuclear Science and Technology*, Taylor and Francis Ltd., **2008**, Vol. 45, pp. 171–174.
- [6] Orano group. Orano Cycle Rapport d'information du site de la Hague, <https://www.orano.group/docs/default-source/orano-doc/groupe/publications-reference/rapport-tsn-la-hague-2019.pdf>, **2019**.
- [7] J. Ahlswede, S. Hebel, J. O. Ross, R. Schoetter, M. B. Kalinowski, *J. Environ. Radioact.* **2013**, 115, 34.
- [8] European commission, EUR-Lex –31996L0029. European directive 31996L0029, **1996**.
- [9] T. B. Borak, J. A. Johnson, *Estimating the Risk of Lung Cancer from Inhalation of Radon Daughters Indoors Review and Evaluation*, **1988**.
- [10] P. Philippe, D. Dafina, *RADON LEVELS IN DWELLINGS*. www.euro.who.int/ENHIS, **2019**.
- [11] R. A. Surette, R. G. C. Mcelroy, *A REVIEW OF TRITIUM-IN-WATER MONITORS*, **1986**.
- [12] P. Theodorsson, *Appl. Radiat. Isot.* **1997**, 50, 311.
- [13] M. Odziomek, F. Chaput, C. Dujardin, F. Lerouge, P. Cassette, M. Sitarz, S. Parola, *ACS Appl. Mater. Interfaces* **2018**, 10, 32304.
- [14] L. E. Kreno, K. Leong, O. K. Farha, M. Allendorf, R. P. Van Duyne, J. T. Hupp, *Chem. Rev.* **2012**, 112, 1105.
- [15] C. Wang, O. Volotskova, K. Lu, M. Ahmad, C. Sun, L. Xing, W. Lin, *J. Am. Chem. Soc.* **2014**, 136, 6171.
- [16] P. L. Feng, et al, in *Nuclear Instruments and Methods in Physics Research, Section A: Accelerators, Spectrometers, Detectors and Associated Equipment*, **2011**, Vol. 652, pp. 295–298.
- [17] J. Perego, I. Villa, A. Pedrini, E. C. Padovani, R. Crapanzano, A. Vedda, C. Dujardin, C. X. Bezuidenhout, S. Bracco, P. E. Sozzani, A. Comotti, L. Gironi, M. Beretta, M. Salomoni, N. Kratochwil, S. Gundacker, E. Auffray, F. Meinardi, A. Monguzzi, *Nat. Photonics* **2021**, 15, 393.
- [18] J. Perego, C. X. Bezuidenhout, I. Villa, F. Cova, R. Crapanzano, I. Frank, F. Pagano, N. Kratochwil, E. Auffray, S. Bracco, A. Vedda, C. Dujardin, P. E. Sozzani, F. Meinardi, A. Comotti, A. Monguzzi, *Nat. Commun.* **2022**, 13.
- [19] J. J. Perryly, et al, *J. Mater. Chem.* **2012**, 22, 10235.
- [20] V. Villemot, N. Dufour, S. Mauree, B. Sabot, G. H. V. Bertrand, M. Hamel, *Adv Photonics Res* **2022**, 3, 2100259.
- [21] B. Sabot, C. Dutsov, P. Cassette, K. Mitev, *Nucl Instrum Methods Phys Res A* **2022**, 1034, 166721.
- [22] B. Sabot, M. Rodrigues, S. Pierre, *Appl. Radiat. Isot.* **2020**, 155, 108934.
- [23] B. Sabot, S. Pierre, P. Cassette, *Appl. Radiat. Isot.* **2016**, 118, 167.
- [24] R. Broda, P. Cassette, K. Kossert, *Metrologia* **2007**, 44.
- [25] G. A. Leith, C. R. Martin, J. M. Mayers, P. Kittikhunnatham, R. W. Larsen, N. B. Shustova, *Chem. Soc. Rev.* **2021**, 50, 4382.
- [26] V. Stavila, A. A. Talin, M. D. Allendorf, *Chem. Soc. Rev.* **2014**, 43, 5994.
- [27] C. R. Martin, P. Kittikhunnatham, G. A. Leith, A. A. Berseneva, K. C. Park, A. B. Greytak, N. B. Shustova, *Nano Res.* **2021**, 14, 338.
- [28] G. H. V. Bertrand, M. Hamel, F. Sguerra, *Chem. - Eur. J.* **2014**, 20, 15660.
- [29] G. H. V. Bertrand, M. Hamel, S. Normand, F. Sguerra, *NIMPR-A* **2015**, 776, 114.
- [30] V. Villemot, M. Hamel, R. B. Pansu, I. Leray, G. H. V. Bertrand, *RSC Adv.* **2020**, 10, 18418.
- [31] S. Pullen, G. H. Clever, *Acc. Chem. Res.* **2018**, 51, 3052.

- [32] H. Furukawa, et al, *Science (1979)* **2010**, 329, 424.
- [33] S. S. Kaye, A. Dailly, O. M. Yaghi, J. R. Long, *J. Am. Chem. Soc.* **2007**, 129, 14176.
- [34] A. Comotti, S. Bracco, P. Valsesia, L. Ferretti, P. Sozzani, *J. Am. Chem. Soc.* **2007**, 129, 8566.
- [35] A. Comotti, S. Bracco, L. Ferretti, M. Mauri, R. Simonutti, P. Sozzani, *Chem. Commun.* **2007**, 350, <https://doi.org/10.1039/b612002d>.
- [36] S. Pawsey, I. Moudrakovski, J. Ripmeester, L.i-Q. Wang, G. J. Exarhos, J. L. C. Rowsell, O. M. Yaghi, *J. Phys. Chem. C* **2007**, 111, 6060.
- [37] H. Li, M. Eddaoudi, M. O'keeffe, O. M. Yaghi, *Nature* **1999**, 402, 276.
- [38] L. M. Santiago, H. Bagán, A. Tarancón, J. F. Garcia, *Nucl Instrum Methods Phys Res A* **2013**, 698, 106.
- [39] K. Mitev, I. Dimitrova, A. Tarancon, D. Pressyanov, L. Tsankov, T. Boshkova, S. Georgiev, R. Sekalova, J. F. Garcia, *IEEE Trans Nucl Sci* **2016**, 63, 1209.
- [40] D. Banerjee, A. J. Cairns, J. Liu, R. K. Motkuri, S. K. Nune, C. A. Fernandez, R. Krishna, D. M. Strachan, P. K. Thallapally, *Acc. Chem. Res.* **2015**, 48, 211.
- [41] J. Sim, H. Yim, N. Ko, S. B. Choi, Y. Oh, H. J. Park, S. Park, J. Kim, *Journal of the Chemical Society. Dalton Transactions* **2014**, 43, 18017.
- [42] A. Vivier, R. Fottorino, B. Rouse, *Radioprotection* **2010**, 45, 321.
- [43] https://318921.fs1.hubspotusercontent-na1.net/hubfs/318921/1_Microsites/French%20Website/Premium/Etendue%20de%20mesure%20d%C3%A9tecteurs%20Premium%20Analyse.pdf.
- [44] <https://www.thermofisher.com/order/catalog/product/fr/en/FHT59E>.
- [45] https://www.berthold.com/fileadmin/DownloadsUnprotected/brochures/Radiation_Protection/Flyer_BAI_9109-4_90861PR2_05.pdf.
- [46] M. A. Kellett, O. Bersillon, in *EPJ Web of Conferences*, EDP Sciences, **2017**, Vol. 146.
- [47] CEA/LNE-LNHB /V. Chisté, M. M. B. LNE-LNHB/CEA-Table de Radionucléides. http://www.lnhb.fr/nuclides/Rn-222_tables.pdf, **2010**.
- [48] H. B. Royal, L. M. Robert, *Anal. Chem.* **1962**, 34, 1122.
- [49] A. Chapon, G. Pigrée, V. Putmans, G. Rogel, *Results Phys* **2016**, 6, 50.
- [50] T. Aoyama, H. Sugiura, T. Watanabe, *Nucl Instrum Methods Phys Res A* **1987**, 254.